Greenhouse gas emissions: A rapid submerge of the world

(Article begins on next page)

26 April 2024

Greenhouse gas emissions: A rapid submerge of the world

A. Gowrisankar, T. M. C. Priyanka, Asit Saha, et al.

View Online   Export Citation   CrossMark

Greenhouse gas emissions: A rapid submerge of the world

View Online   Export Citation   CrossMark

A. Gowrisankar,[1] T. M. C. Priyanka,[1] Asit Saha,[2] Lamberto Rondoni,[3,4] (iD) Md. Kamrul Hassan,[5] (iD)
and Santo Banerjee[3,a)] (iD)

AFFILIATIONS

[1] Department of Mathematics, School of Advanced Sciences, Vellore Institute of Technology, Vellore 632 014, Tamil Nadu, India
[2] Department of Mathematics, Sikkim Manipal Institute of Technology, Sikkim Manipal University, Majitar, Rangpo 737136, East Sikkim, India
[3] Dipartimento di Scienze Matematiche, Politecnico di Torino, Corso Duca degli Abruzzi, 24, 10129 Torino, Italy
[4] INFN, Sezione di Torino, Via P. Giuria 1, 10125 Torino, Italy
[5] Theoretical Physics Group, Department of Physics, University of Dhaka, Dhaka 1000, Bangladesh

[a)] **Author to whom correspondence should be addressed:** santoban@gmail.com

ABSTRACT

The investigation of worldwide climate change is a noticeable exploration topic in the field of sciences. Outflow of greenhouse gases in the environment is the main reason behind the worldwide environmental change. Greenhouse gases retain heat from the sun and prompt the earth to become more sultry, resulting in global warming. In this article, a model based technique is proposed to forecast the future climate dynamics globally. Using past data on annual greenhouse gas emissions and per capita greenhouse gas emissions, the fractal curves are generated and a forecast model called the autoregressive integrated moving average model has been employed to anticipate the future scenario in relation to climate change and its impact on sea-level rise. It is necessary to forecast the climate conditions before the situations become acute. Policy measures aimed at lowering CO_2 and other greenhouse gas emissions, or at least slowing down their development, will have a substantial effect on future warming of the earth.

Human requirements are increasing day by day, driving him to think faster and invent things much faster, thus resulting in the world updates. Though the upgrades are helpful for an easy and more convenient lifestyle, they also lead to drastic changes in the environment. In many aspects, the changes are worldwide. One such prominent change is climate change. This change is the result of greenhouse gas emissions and is extremely harmful, as one of its key consequences is sea level rise. This paper addresses the global climate change and forecasts future greenhouse gas emission rates using fractal interpolation and the autoregressive integrated moving average (ARIMA) model and, as a result, creates awareness for the need to reduce global greenhouse gas emissions and thus prevent the submerge of the world.

I. INTRODUCTION

Long-term changes in temperature and weather conditions are referred to as climate change. Extreme weather occurrences (such as floods, storms, and droughts), sea-level rise, and interrupted water systems are just a few of the ecological, physical, and health consequences of a changing climate. Natural reasons, such as solar cycle oscillations, could cause climate change patterns. However, anthropogenic activities have been a significant cause for the modern climate era since 1800s, owing to the combustion of fossil fuels, such as gas, coal, and oil. Fossil fuel combustion leads to emission of greenhouse gases, which act as a shield over the earth, capturing the sun's heat and increasing temperatures. Nitrous oxide (N_2O), carbon dioxide (CO_2), water vapor, methane (CH_4), and chlorofluorocarbons are all the gases that lead to the greenhouse effect, and CO_2 is the most abundant one of these greenhouse gases. Greenhouse gases (GHG) are necessary to keep the earth warm; without them, the average temperature would be around $0°F$. Human activities, such as clearing of land for agriculture, industry, and others, have increased the concentrations of greenhouse gases in the atmosphere. This results in atmospheric warming and global climate change; refer to Fig. 1. More details on the connection between the
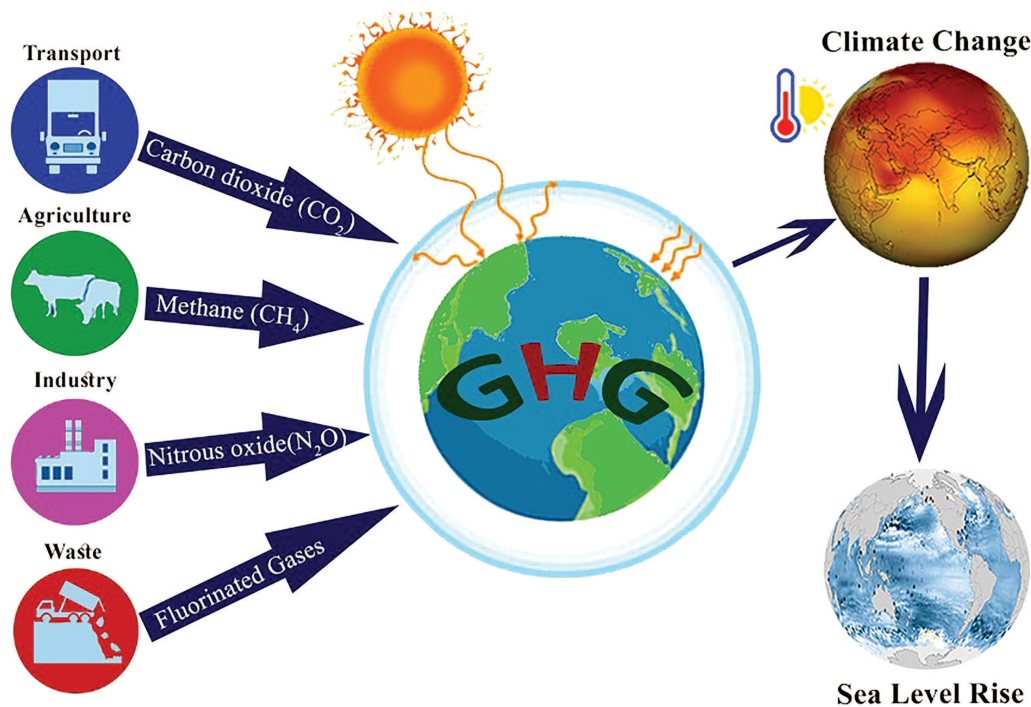
FIG. 1. Effect of GHG emissions in climate change.

greenhouse gases and climate change can be found in the literature.[1,2] Ren *et al.* have discussed the GHG emissions due to on-site fuel consumption using home equipment, and appliances are calculated for the household energy consumption.[3] Susanne *et al.* have introduced the climate tipping impact category to represent the climate tipping potential (CTP) of GHG emissions relative to a climatic target level and have discussed the urgent impacts of GHG emissions.[4] Nguyen *et al.* have discussed the environmental impacts and greenhouse gas emissions for energy recovery of the wastewater treatment plant.[5]

Since from the beginning, life is a delicate balance with the sea level. The greenhouse gas emissions has thrown the system out of balance by elevating sea levels. By melting mountain glaciers, forcing ice sheets to melt into the oceans and expanding ocean water, greenhouse gas emissions will raise sea levels by a few meters in the next century and several meters in the following few hundred years.[6] A rise of this magnitude would start flooding deltas and other coastal lowlands, degrade beaches, and endanger aquifer water quality. Hence, it is generally acknowledged that the world must reduce greenhouse gas emissions as quickly as possible to avoid the submerge of the world. To escape from severe climate change, global greenhouse gas emissions should be reduced rapidly. Every year, the world emits roughly 50×10^9 tons of greenhouse gases. To ascertain how to reduce the emissions effectively and with the aid of current technologies, what emissions could and could not be eliminated, it is important to understand where the emissions come from. Energy (electricity, heat, and transport), industrial processes, and waste and land use (agriculture and forestry) are the primary

sectors causing greenhouse gas emissions. Monitoring the global temperature changes on a global scale is essential; in the meantime, we need to be aware of how warming is spread unevenly around the world. In some areas, warming is extremely more intense. The level
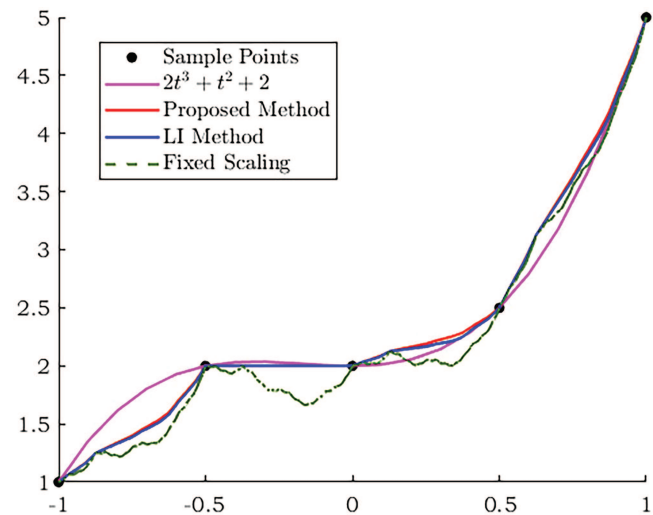

FIG. 2. Approximation of $2t^3 + t^2 + 2$ using three various scaling factors l_j, l_j^*, and l_j^{**}.
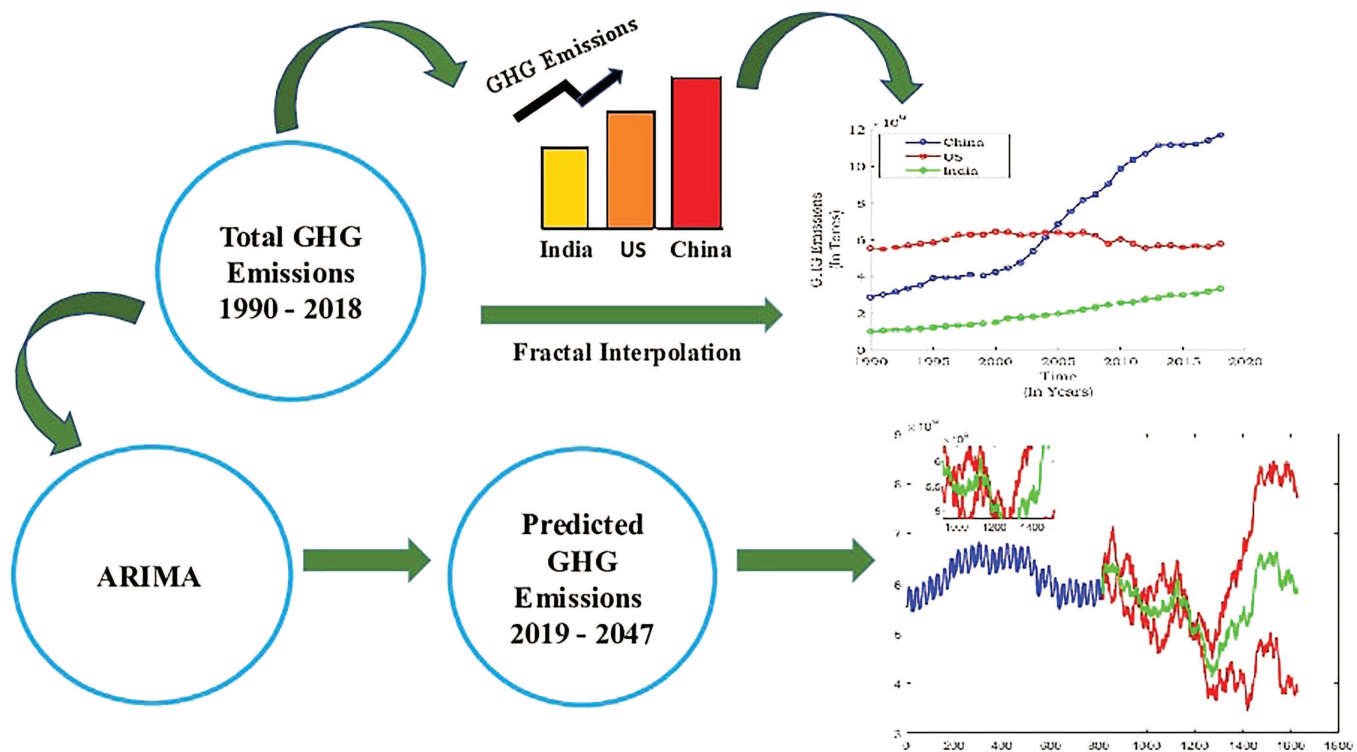
FIG. 3. Schematic representation of the proposed model.

of greenhouse gases released into the atmosphere varies by country. China produces the most greenhouse gas emissions of any nation in the globe. The United States is the world's second-largest emitter of carbon dioxide. India, like China, has a vast population and is the third-largest CO_2 emitter in the world. A substantial greenhouse effect would warm the ocean and cause glaciers to melt partially, increasing sea levels. Due to its heat, ocean will also expand, further accelerates rise in sea level. Perhaps, a little rise in sea level can have a major influence on many coastal areas, some of which can have a variety of effects on both human health as well as water resource accessibility. The forecast of greenhouse gas emissions from the industries in India and China has been investigated.[7] Six different interpolation methods have used to investigate rainfall patterns under varying climatic conditions in the Chongqing province.[8] Fractal properties of climate change in northwest China over the past 50 years have studied.[9] The impact of sea-level rise on the coastal groundwater discharge as a result of climate change is discussed by Masciopinto and Liso.[10] Authors have utilized the fractal dimensional analysis to explore the Indian climatic dynamics.[11] The studies relating the interpolation for the forecast of greenhouse gas emissions and other time series problems are also explored in the literature.[12–16] The aim of the study is to forecast the future climate conditions of the world by investigating the annual GHG emissions of three most greenhouse gas emitting countries: China, USA, and India. Also, by examining the per capita GHG emissions

of 11 countries: Botswana, Canada, Australia, Saudi Arabia, United States, Germany, Russia, China, United Kingdom, Brazil, and India, future per capita GHG emissions are predicted. The world's largest emitters are inferred by total annual emissions of greenhouse gases. However, the population of a country also primarily accounts for the greenhouse gas emissions. For instance, China and India are the top three emitters as well as the world's two most populous countries. The per capita greenhouse gas emissions of a country are measured in tons per person per year. Among the major emitters, large differences can be observed in the per capita emissions: in the US, the average person emits more than 18 tons; in China, it is less than half, at 8 tons; and in India, emissions are much lower, at roughly 2.5 tons. As the world's smaller countries, such as Botswana and others, tend to be large oil and/or gas producing countries, they fall under the category of largest per capita GHG emitters. The aforementioned reason made us to choose the particular 11 countries: which are the top 11 per capita emitters based on the evidences of Our World in Data.[17]

An advanced interpolation technique called the fractal interpolation finds its applications in many other areas of science, beyond the interpolation and approximation theory, due to its self-similarity characteristic and scale invariance properties. For example, Wang *et al.* have explored the forecasting stock price indexes using fractal interpolation.[18] To improve the neural network predictions for complicated time series data, fractal interpolation approach has been
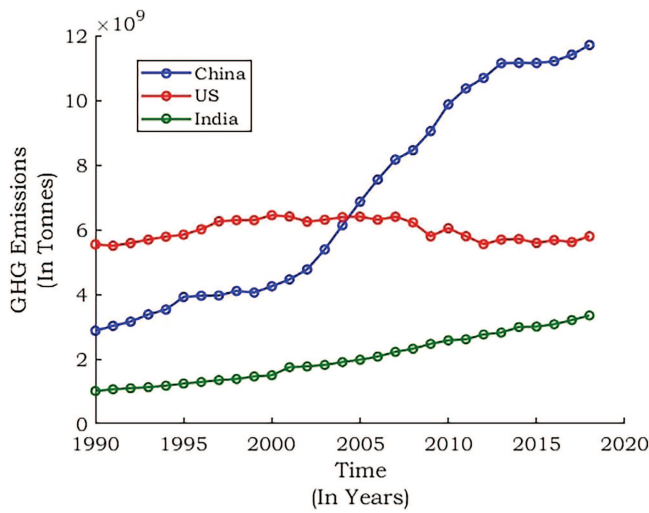
FIG. 4. Total GHG emissions.

employed by Raubitzek and Neubauer.[19] Xiu *et al.* have developed a short-term prediction method for wind speed series by utilizing the fractal interpolation.[20] Recently, Gowrisankar *et al.* have predicted the trend of an Omicron variant with the help of a fractal interpolation technique.[21]

The ultimate aim of this research is to create public awareness about the negative consequences of greenhouse gas emissions, notably sea-level rise. However, while many research studies have been conducted to address global warming and its consequences, only a few of them have used data-driven methodologies. In the

present work, to preprocess and forecast the chaotic nature of greenhouse gas emissions, we were using a data-driven approach with a combination of fractal interpolation and the ARIMA model as the core principle of analysis. As a result, we are highly confident that the current study is one of the most fascinating and timely studies on global greenhouse gas emissions and their impact. In this study, using the fractal interpolation method, the sample data on GHG emissions have been reconstructed. By studying variations in the scaling properties, fractal analysis yields a novel method to better approximate the climate data. For more details of fractal functions and its recent advancements, the reader is recommended to refer Refs. 22–29. In addition, with the aid of the ARIMA model, the predictions are performed from the year 2019–2047 for the preprocessed sample data.

The rest of the article is organized as follows. Section I provides the introduction of the present work. Section II discusses the construction of a linear fractal function with a numerical illustration. Furthermore, the ARIMA model is described, and the fractal interpolation–ARIMA algorithm and evaluation metrics, such as MAPE, NMAPE, and RMSE, are discussed in Sec. II. The collection of data for the present work is discussed in Sec. III. Section IV is devoted to the results and discussion part of the study. The concluding remarks of the proposed model for forecasting the future climatic conditions are presented in Sec. V.

II. METHODS AND MATERIALS

A. Construction of a linear fractal interpolation function

A fractal interpolation function is generally constructed using the iterated function system as a graph of continuous function interpolating the given two-dimensional data set. An iterated function system is a pair consisting of a complete metric space along with
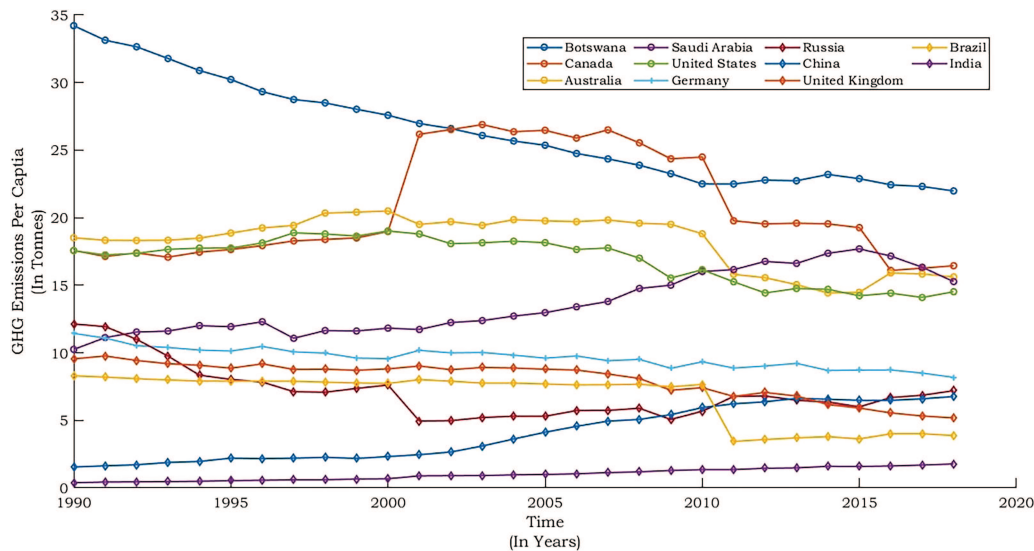

FIG. 5. Per capita greenhouse gas emissions.

FIG. 6. Comparison of predicted greenhouse gas emissions (in tons) from 2019 to 2047 using ARIMA (1,1,1) with scaling factors l_j: (a) China, (b) US, (c) India, and (d) World.

a finite number of contraction maps. The deterministic fractal or attractor is obtained as the unique fixed point of the IFS.

Consider the data set $\{(t_i, u_i) \in \mathbb{R}^2 : j \in \{0, 1, \ldots, N\}\}$ such that $t_{j-1} < t_j$ for all $j = 1, 2, \ldots, N$. Let $I = [t_0, t_N]$ be the closed interval of $\mathbb{R}$ and set $I_j = [t_{j-1}, t_j]$. Let $L_j : I \to I_j$ be the contractive homeomorphisms and for all $t, t' \in I$, $r_j \in (0, 1)$ obeys

$$|L_j(t) - L_j(t')| \le r_j|t - t'|, \; L_j(t_0) = t_{j-1}, \; L_j(t_N) = t_j.$$

Let $F_j : X \subset I \times \mathbb{R} \to \mathbb{R}$ be N continuous mappings and contraction with respect to a second variable such that for all $z, z' \in \mathbb{R}$, $t \in I$ and $s_j \in (-1, 1)$ satisfies the conditions

$$|F_j(t, z) - F_j(t, z')| \le s_j|z - z'|, F_j(t_0, z_0) = z_{j-1}, F_j(t_N, z_N) = z_j.$$

Define the maps $f_j : X \to I_j \times \mathbb{R}, j = 1, \ldots, N$ by

$$f_j(t, u) = (L_j(t), F_j(t, u)).$$

Let $H(X)$ and ρ denote the collection of all non-empty compact sets of X and Hausdorff metric, respectively. The function $F : H(X) \to H(X)$ is defined as the finite union of contraction mappings $f_j(C)$, where $C \in H(X)$. As the space $(H(X), \rho)$ is a complete metric space, then by the Banach contraction theorem, the map F has a unique invariant compact set, say G, such that $F(G) = G$ and $G = lim_{n \to \infty} F^{\circ n}(C)$. This invariant set G is the graph of the continuous function f satisfying $f(t_j) = u_j$ for $j = 0, 1, \ldots, N$ and is termed as the fractal interpolation function for the IFS $\{X; f_j : j = 1, 2, \ldots, N\}$.
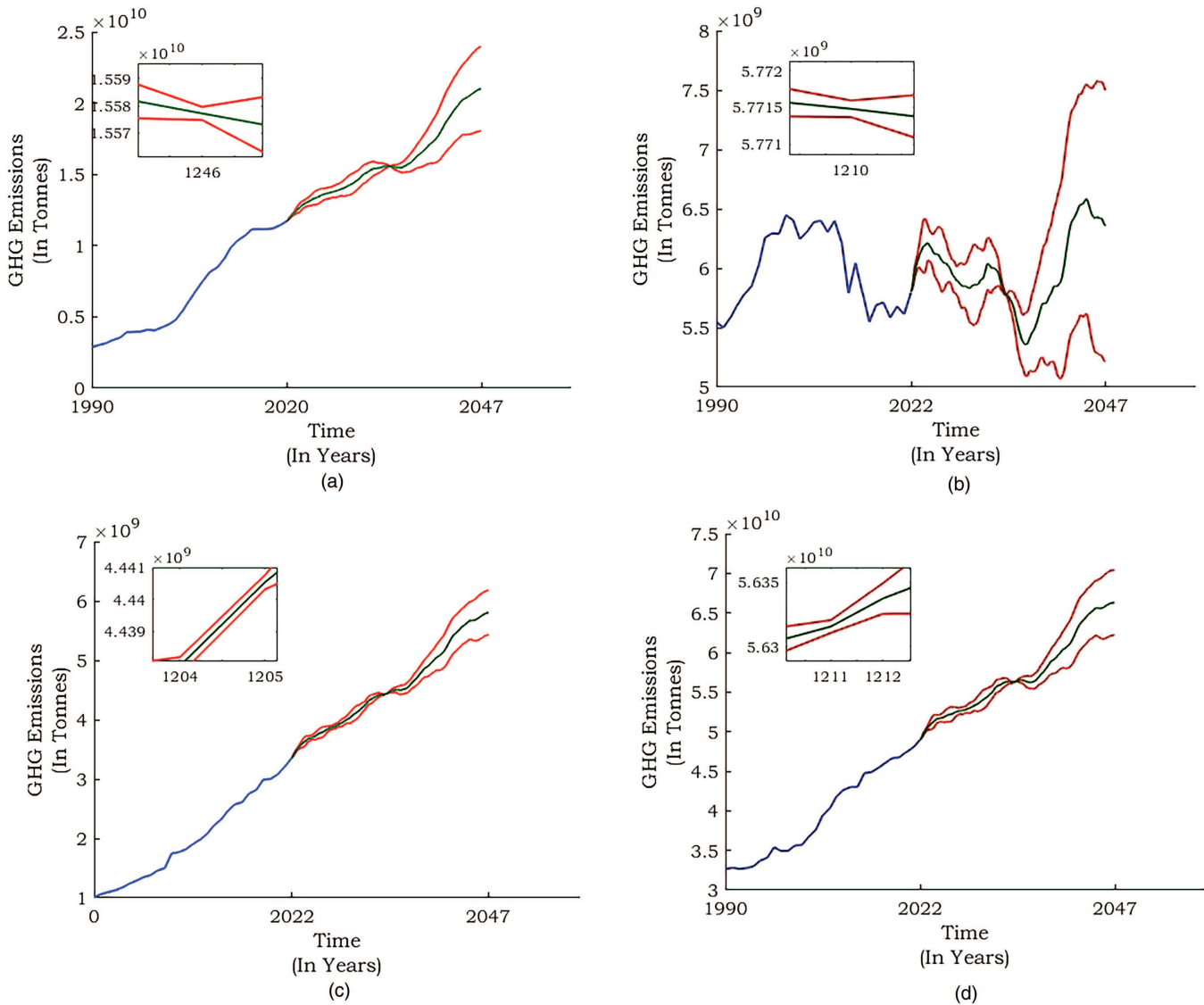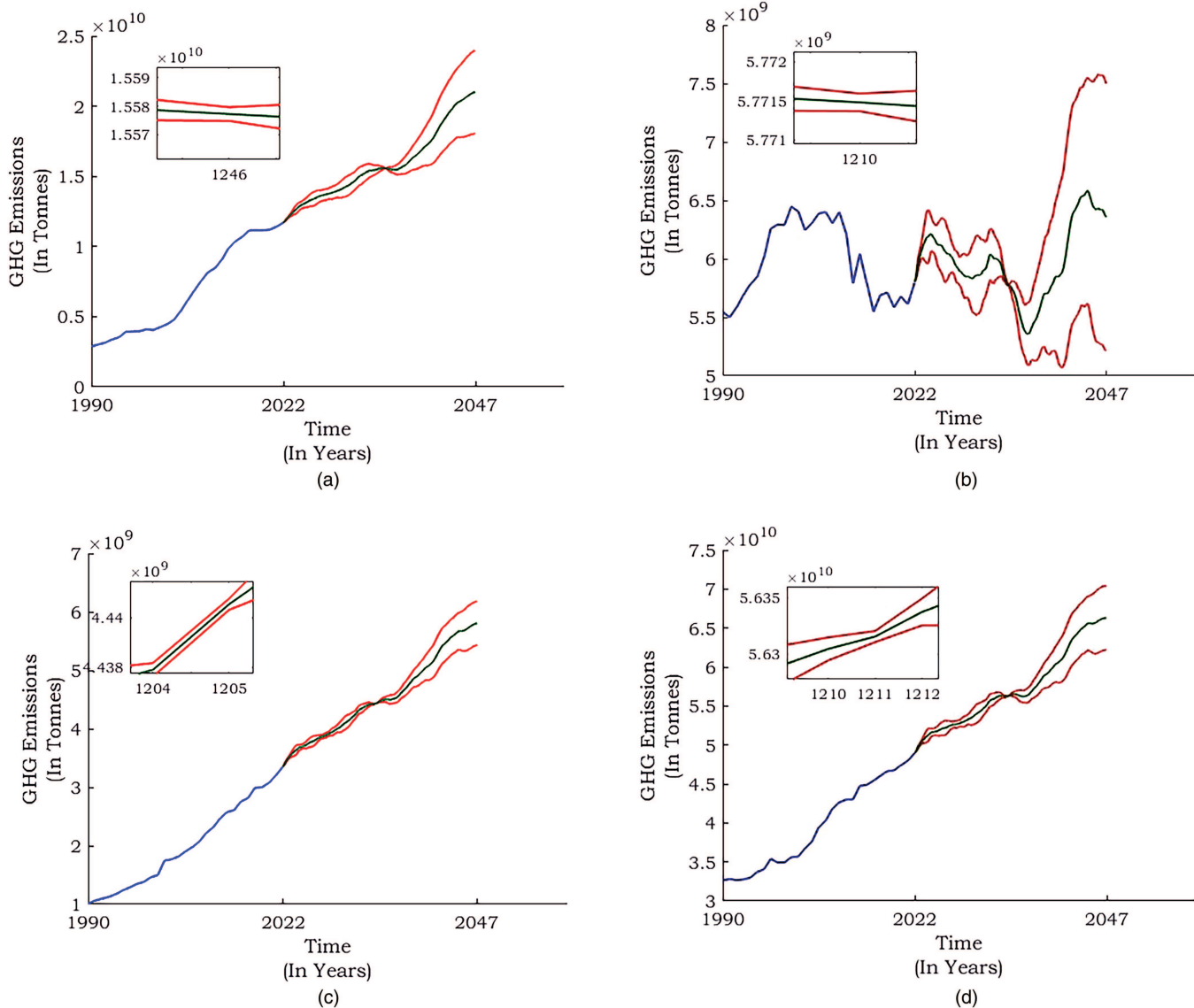
FIG. 7. Comparison of predicted greenhouse gas emissions (in tons) from 2019 to 2047 using ARIMA (1,1,1) with scaling factors l_j^*: (a) China, (b) US, (c) India, and (d) World.

Based on the self-similar nature of the data, the reconstruction of data can be done by the fractal function approach. For generating such a fractal function, a suitable iterated function system must be built. The fractal features of its attractor are similar to those of the expected data in this so-called suitable iterated function system. Concretely, the attractor's trajectory should be close enough to the observed data. Since only the scaling factors can be utilized to build a suitable iterated function system, this is acceptable for the sample distribution.

This paper investigates the prediction of future climatic conditions; we, therefore, consider the finite two-dimensional data set $\{(t_j, u_j) : j = 0, 1, \ldots, N\}$, where t_j denotes the time period

(in years) and u_j denotes the GHG emissions (in tons). The following affine transformation is considered to construct the required linear fractal interpolation function:

$$\begin{pmatrix} t \\ u \end{pmatrix} \rightarrow v_j \begin{pmatrix} t \\ u \end{pmatrix} = \begin{pmatrix} m_j & 0 \\ n_j & l_j \end{pmatrix} \begin{pmatrix} t \\ u \end{pmatrix} + \begin{pmatrix} p_j \\ q_j \end{pmatrix}. \quad (1)$$

That is, $(t, u) \rightarrow (m_j t + p_j, n_j t + l_j u + q_j)$, and each contraction map v_j satisfies the conditions

$$v_j \begin{pmatrix} t_0 \\ u_0 \end{pmatrix} = (t_{j-1}, u_{j-1}), \, v_j \begin{pmatrix} t_N \\ u_N \end{pmatrix} = (t_j, u_j) \quad (2)$$
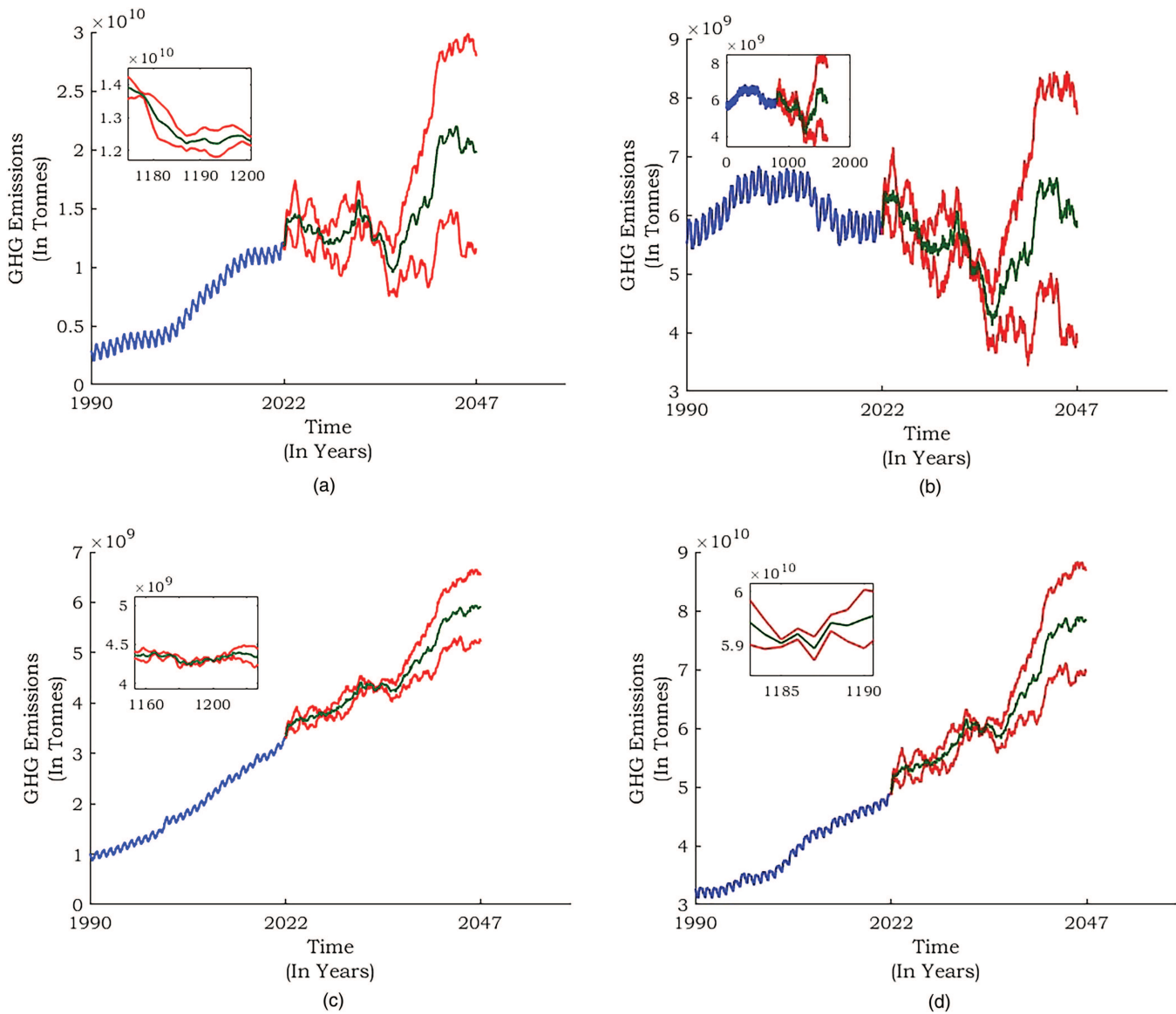
FIG. 8. Comparison of predicted greenhouse gas emissions (in tons) from 2019 to 2047 using ARIMA (1,1,1) with scaling factors l_j^{**}: (a) China, (b) US, (c) India, and (d) World.

for all $j = 1, 2, \ldots, N$, m_j, n_j, l_j, p_j, q_j are the real parameters, and l_j are the vertical scaling factors and also called as contraction factors for the contraction maps v_j. Note that l_j can be chosen as free variables such that $l_j \in (-1, 1)$. Using the system of linear equations (2), the other parameters are determined as

$$m_j = \frac{t_j - t_{j-1}}{t_N - t_0},$$

$$p_j = \frac{t_N t_{j-1} - t_0 t_j}{t_N - t_0},$$

(3)

$$n_j = \frac{(u_j - u_{j-1}) - d_j(u_N - u_0)}{t_N - t_0},$$

$$q_j = \frac{(t_N u_{j-1} - t_0 u_j) - d_j(t_N u_0 - t_0 u_N)}{t_N - t_0}$$

for $j = 1, 2, \ldots, N$. The fluctuation of the interpolation curve along the vertical direction is greatly influenced by the scaling factor l_j. Therefore, in this study, the linear interpolation function is constructed to recreate the data by choosing the scaling factors l_j appropriately as discussed in Sec. II B. A variety of interesting fractals
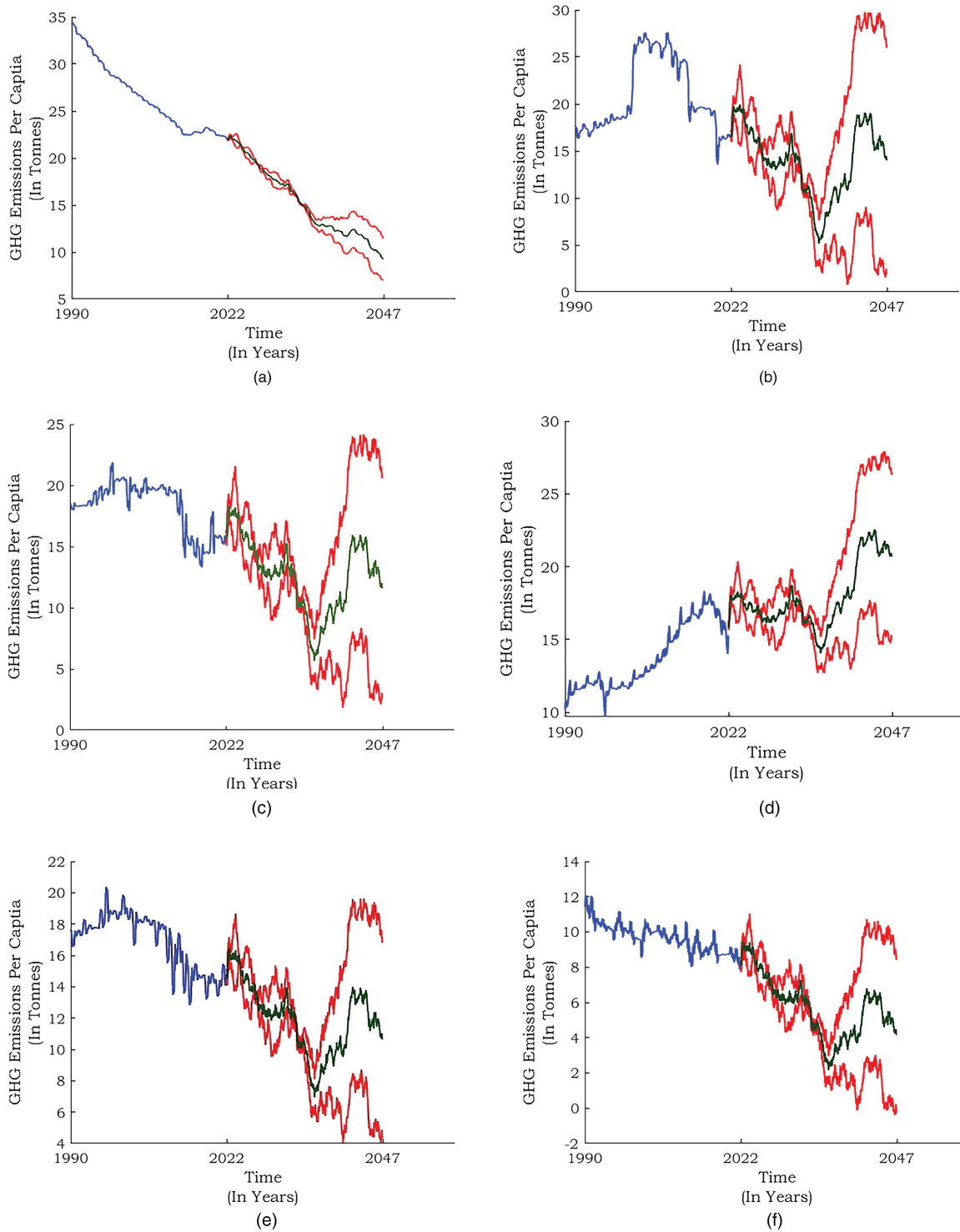
FIG. 9. Comparison of predicted per capita greenhouse gas emissions (in tons) from 2019 to 2047 using ARIMA (1,1,1) with scaling factors l_j: (a) Botswana, (b) Canada, (c) Australia, (d) Saudi Arabia, (e) USA, and (f) Germany.
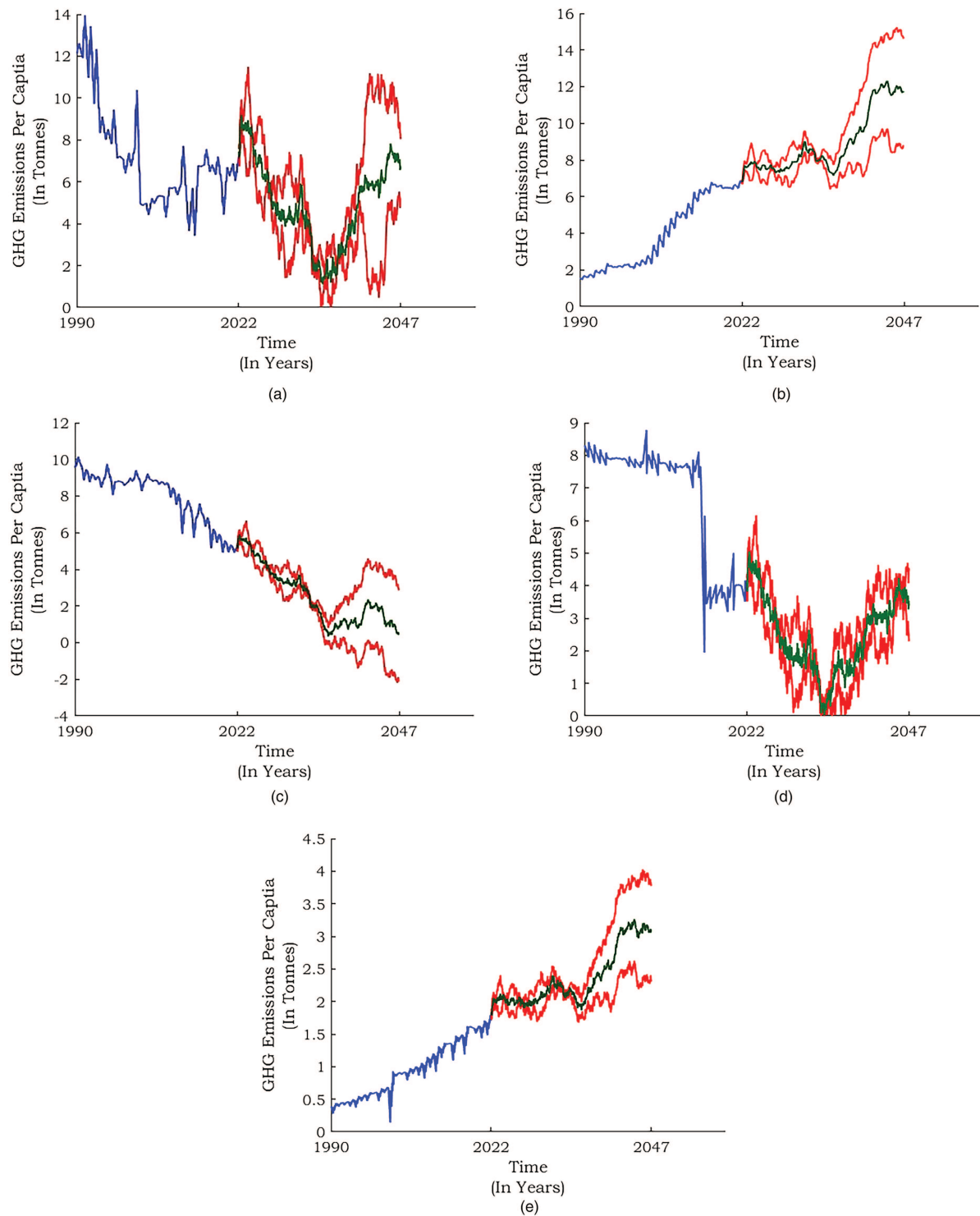
FIG. 10. Comparison of predicted per capita greenhouse gas emissions (in tons) from 2019 to 2047 using ARIMA (1,1,1) with scaling factors l_j: (a) Russia, (b) China, (c) UK, (d) Brazil, and (e) India.

TABLE I. Evaluation of forecast errors through MAPE, NMAPE, and RMSE values of 11 countries for three models: Model I (l_j), Model II (l_j^*), and Model III (l_j^{**}).

Country	Model - I			Model - II			Model - III		
	MAPE	NMAPE	RMSE	MAPE	NMAPE	RMSE	MAPE	NMAPE	RMSE
Botswana	0.4021	0.4097	10.8174	0.4118	0.4199	11.1285	0.4093	0.4199	10.9284
Canada	0.3592	0.3338	9.4218	0.3778	0.3499	9.7681	0.5871	0.5820	17.4758
Australia	0.2601	0.2523	5.1387	0.3198	0.3152	6.9172	0.3834	0.3788	8.7035
Saudi Arabia	0.2899	0.3080	4.3852	0.2870	0.3035	4.5116	0.0925	0.1891	3.0163
USA	0.2238	0.2189	4.0565	0.2977	0.2909	5.6103	0.3190	0.3125	6.1007
Germany	0.3282	0.3314	3.2258	0.4052	0.4092	4.2254	0.3507	0.3542	3.5218
Russia	0.3087	0.3288	2.5793	0.4521	0.4914	3.8194	0.4058	0.5416	4.0141
China	1.0244	1.3114	5.2775	0.9609	1.2437	5.0409	0.8820	1.1672	4.8980
UK	0.6681	0.6827	5.5821	0.6673	0.6794	5.5341	0.7030	0.7143	6.1644
Brazil	0.8590	0.8741	6.3005	0.8249	0.8385	5.9644	0.8224	0.8361	6.2146
India	0.7879	1.0424	1.0787	1.2289	1.4873	1.4244	1.2469	1.5033	1.4529

in the real-world occur as graphs of functions. Calculating fractal dimension for the fractal interpolation functions aids to recognize the irregularity of the curves. The fractal dimension D of any fractal object can be estimated using the power law (fractal scaling law) $N = R^{-D}$, where N is the number of parts that the object gets divided up and R is the size of the parts (scaling factor). One of the most important properties of the power law is scaling invariance. In this study, the fractal curves of total GHG emissions and per capita GHG emissions predicted for various countries obey the fractal scaling law. As mentioned earlier, the vertical scaling factor determines the shape and pattern of the fractal interpolation function. In precise, the evolution of reconstructing fractal function depends on the scaling factors. Hence, the present study includes the comparative analysis of different types of scaling factors, which are involved in the prediction scheme.

B. Numerical illustration

Let us construct a linear fractal interpolation function, which passes through the four data points: $\{(t_0; u_0) = (-1, 1), (t_1; u_1) = (-1/2, 2), (t_2; u_2) = (0, 2), (t_3; u_3) = (1/2, 5/2), (t_4; u_4) = (1, 5)\}$. The IFS containing four contraction maps $\{v_1, v_2, v_3, v_4\}$ can be generated using the given interpolation points. Each F_i is a affine transformation as in Eq. (1). The unknown parameters of the maps v_i are determined as follows:

$$m_j = \frac{t_j - t_{j-1}}{t_N - t_0} = \frac{1}{4},$$

$$p_j = \frac{t_N t_{j-1} - t_0 t_j}{t_N - t_0} = \frac{t_{j-1} + t_j}{2},$$

$$n_j = \frac{(u_j - u_{j-1}) - l_j(u_N - u_0)}{t_N - t_0} = \frac{u_j - u_{j-1} - 4l_j}{2},$$

$$q_j = \frac{(t_N u_{j-1} - t_0 u_j) - l_j(t_N u_0 - t_0 u_N)}{t_N - t_0} = \frac{u_{j-1} + u_j - 6l_j}{2}. \quad (4)$$

Now, substituting all the above determined values into Eq. (1), one can get the special structure shown below:

$$v_j \begin{pmatrix} t \\ u \end{pmatrix} = \begin{pmatrix} 1/4 & 0 \\ \frac{u_j - u_{j-1} - 4l_j}{2} & l_j \end{pmatrix} \begin{pmatrix} t \\ u \end{pmatrix} + \begin{pmatrix} \frac{t_{j-1}+t_j}{2} \\ \frac{u_{j-1}+u_j-6l_j}{2} \end{pmatrix}. \quad (5)$$

By fixing the value of vertical scaling factors l_j to $1/2$ for all $j = 1, 2, 3, 4$, the four affine maps are expressed as

$$v_1 \begin{pmatrix} t \\ u \end{pmatrix} = \begin{pmatrix} 1/4 & 0 \\ -1/2 & 1/2 \end{pmatrix} \begin{pmatrix} t \\ u \end{pmatrix} + \begin{pmatrix} -3/4 \\ 0 \end{pmatrix},$$

$$v_2 \begin{pmatrix} t \\ u \end{pmatrix} = \begin{pmatrix} 1/4 & 0 \\ -1 & 1/2 \end{pmatrix} \begin{pmatrix} t \\ u \end{pmatrix} + \begin{pmatrix} -1/4 \\ 1/2 \end{pmatrix},$$

$$v_3 \begin{pmatrix} t \\ u \end{pmatrix} = \begin{pmatrix} 1/4 & 0 \\ 3/4 & 1/2 \end{pmatrix} \begin{pmatrix} t \\ u \end{pmatrix} + \begin{pmatrix} 1/4 \\ 3/4 \end{pmatrix},$$

$$v_4 \begin{pmatrix} t \\ u \end{pmatrix} = \begin{pmatrix} 1/4 & 0 \\ 1/4 & 1/2 \end{pmatrix} \begin{pmatrix} t \\ u \end{pmatrix} + \begin{pmatrix} 3/4 \\ 9/4 \end{pmatrix}.$$

Each map generates five new data points after each iteration when the given five points are sequentially substituted in the above four affine maps.

A complex interpolation graph can be produced by raising the number of iterations. The interpolation curve formed by the IFS has fractal properties, and it is rough in any segment. This is in stark contrast to the smooth curve produced by the conventional interpolation approach. The function value at any $t \in (0, 1)$ can be deduced using this fractal curve.

In Fig. 2, the black dots represent the sample data points, $\{(-1, 1), (-1/2, 2), (0, 2), (1/2, 5/2), (1, 5)\}$, and the pink curve is the original function $2t^3 + t^2 + 2$. The original function is approximated using the fractal interpolation method in three ways. The red curve is drawn using the scaling factor l_j, which is proposed in the present paper. The blue curve approximation is done by choosing the scaling factor

$$l_j^* = \frac{y_j - y_{j-1}}{\delta\sqrt{(y_{max} - y_{min})^2 + (y_j - y_{j-1})^2}}$$
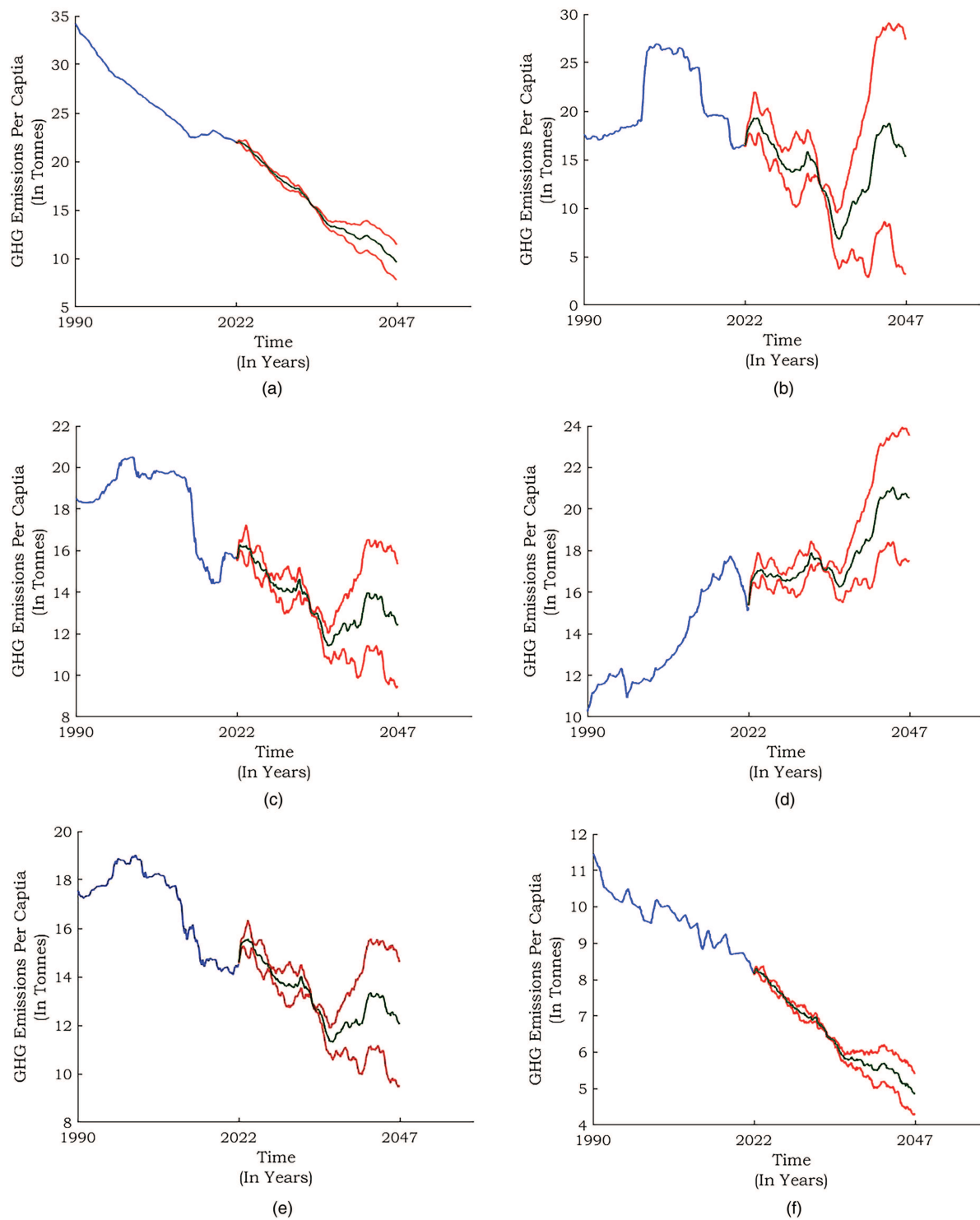
FIG. 11. Comparison of predicted per capita greenhouse gas emissions (in tons) from 2019 to 2047 using ARIMA (1,1,1) with scaling factors l_j^*: (a) Botswana, (b) Canada, (c) Australia, (d) Saudi Arabia, (e) USA, and (f) Germany.

taken from the literature,[14] and it is named as the *LI method* of approximation, where $\delta = 1 + \text{rand}(\varepsilon)$ and the $\text{rand}(\varepsilon)$ represents the number randomly taken by the computer. Furthermore, the green dotted curve in Fig. 2 represents the approximation using the constant scaling factor $l_j^{**} = 1/2$. The statistical significance of the three models has been verified using the evaluation metric, root mean square error (RMSE). It is observed that the RMSE values for the three models I, II, and III are 0.150, 0.170, and 0.2111, respectively. This clearly shows that the red curve drawn using the proposed method (model I) with the scaling factor l_j is the best approximation to the original (pink) curve among the three models.

C. ARIMA

The autoregressive integrated moving average (ARIMA) is a short-term time series forecasting model, which has been increasingly utilized since the development of powerful statistical software packages. This model has been developed using the mathematical approach in order to describe and analyze the variations on the time series. Furthermore, it is designed in such a way to minimize the difference between the observed and estimated values near zero. Employing this approach, the behaviors of both stationary and non-stationary series can be addressed. Autoregressive terms in the forecasting equation are lags of the differenced series, moving average terms are lags of the forecast errors, and an integrated version of a stationary series is a time series that needs to be differenced to make it stationary. The ARIMA model is decomposed into three model parameters; namely, AR (p), I (d), and MA (q), all together form ARIMA (p, d, q) model, where

$$p = \text{order of the autoregressive model,}$$

$$d = \text{degree of differencing,}$$

$$q = \text{order of moving averages,}$$

Autoregressive (AR) denotes the autoregressive variables, Integrated (I) denotes the data values that have been changed with the difference between their actual values and their former values, and the Moving Average (MA) denotes the linear trend of error terms.

A non-seasonal stationary time series can be designed by combining the past values and the errors, which can be represented as ARIMA (p, d, q),

$$Y_t = c + \beta_1 Y_{t-1} + \beta_2 Y_{t-2} + \cdots + \beta_p Y_{t-p} + e_t - \alpha_1 e_{t-1}$$
$$- \alpha_2 e_{t-2} - \cdots - \alpha_q e_{t-q},$$

where c is a constant, Y_t are actual values at time t, e_t are random errors at time t, α_k and β_l are model parameters for $k = 1, 2, \ldots, p$ and $l = 1, 2, \ldots, q$, and p and q are orders of autoregressive and moving average polynomials.

D. Fractal interpolation–the ARIMA algorithm

The algorithm for the construction of IFS corresponding to the given data set is as follows:

(1) Let $D = \{(t_j, u_j) \in \mathbb{R}^2 : j \in \{0, 1, \ldots, N\}\}$ be the sample data where t_j and u_j denote the time period (year) and the rate of greenhouse gas emissions in tons, respectively, at rough scales.

(2) All data points in set D are considered points of interpolation to fully reflect the overall variation pattern. The set D contains $n + 1$ data points that can be splitted into n intervals of interpolation.
(3) Consider the first element and the next element in D as the initial and end points of the interpolation interval.
(4) Calculate the parameters m_j and p_j in (3) for the given sample.
(5) The parameter l_j is calculated using the formula

$$l_j = \frac{y_j - y_{j-1}}{\frac{\Delta y}{\Delta x} \sqrt{(y_{\max} - y_{\min})^2 + (y_j - y_{j-1})^2}},$$

where $\Delta y = y_{\max} - y_{\min}$, $\Delta x = x_{\max} - x_{\min}$; $y_{\max}$ and $y_{\min}$ are the maximum and minimum values of GHG emissions, respectively.
(6) Calculate the parameters n_j and q_j using l_j in the above step and (3).
(7) Next, take the end point of the first interpolation interval as the initial point of the next interpolation interval and iterate the steps (1)–(6) to obtain the IFS $\{X; f_j : j = 1, 2, \ldots, N\}$ for the sample D. By obtaining the fractal curves using the IFS constructed in the step (7), the sample data set is reconstructed. Now, on applying the ARIMA model over the reconstructed new data set, the future data points are predicted. The schematic representation of the proposed algorithm is presented in Fig. 3.

E. Evaluation metrics

In this study, the mean absolute percentage error (MAPE), the normalized mean absolute percentage error (NMAPE), and the root mean square error (RMSE) are used as evaluation metrics to estimate the error. For many sorts of energy forecasts, the MAPE and NMAPE are the most often used fit metrics since both can be converted to accuracy with ease (that is, in terms of percentage). RMSE is another frequently used metric to evaluate the deviation of the estimated values from the observed values. Let $y(t_j) = \{y(t_1), y(t_2), \ldots, y(t_N)\}$ denote the given sample (observed) data and $\hat{y}(t_j) = \{\hat{y}(t_1), \hat{y}(t_2), \ldots, \hat{y}(t_N)\}$ represents the estimated (preprocessed) data of the sample using the fractal interpolation technique. The formulations of MAPE, NMAPE, and RMSE are given below:

$$\text{MAPE (\%)} = \frac{1}{N} \sum_{j=1}^{N} \left| \hat{y}(t_j) - y(t_j) \right| \times 100\%, \tag{6}$$

$$\text{NMAPE (\%)} = \frac{1}{N} \sum_{j=1}^{N} \left| \frac{y(t_j) - \hat{y}(t_j)}{\frac{1}{N} \sum_{j=1}^{N} y(t_j)} \right| \times 100\%. \tag{7}$$

In order to interpret the MAPE (%) values, a scale has been developed by C. D. Lewis, known as the Lewis scale, in 1982. According to this scale, the forecast that is closer to 50% is regarded as the reasonable forecast. This would have made sense in the 1980s, while the modeling and forecasting were not as sophisticated as they are now. In today's world, any decision maker may consider a 50% error as a reasonable forecast while making a critical decision. Meanwhile, the advancements in the forecasting methods and knowledge are constantly driving the accuracy bounds higher. Over the previous three decades, time series prediction has significantly improved.
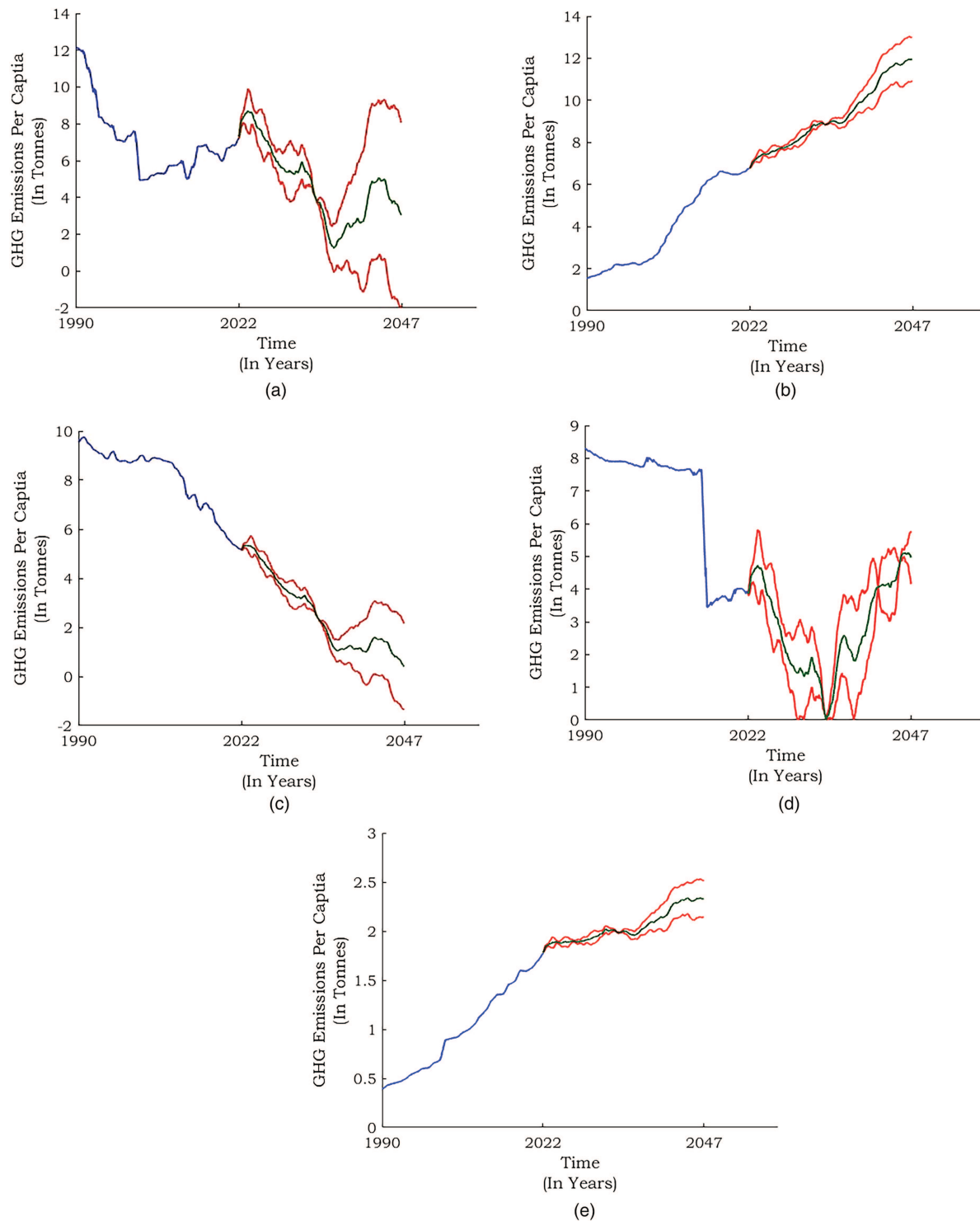
FIG. 12. Comparison of predicted per capita greenhouse gas emissions (in tons) from 2019 to 2047 using ARIMA (1,1,1) with scaling factors l_j^*: (a) Russia, (b) China, (c) UK, (d) Brazil, and (e) India.
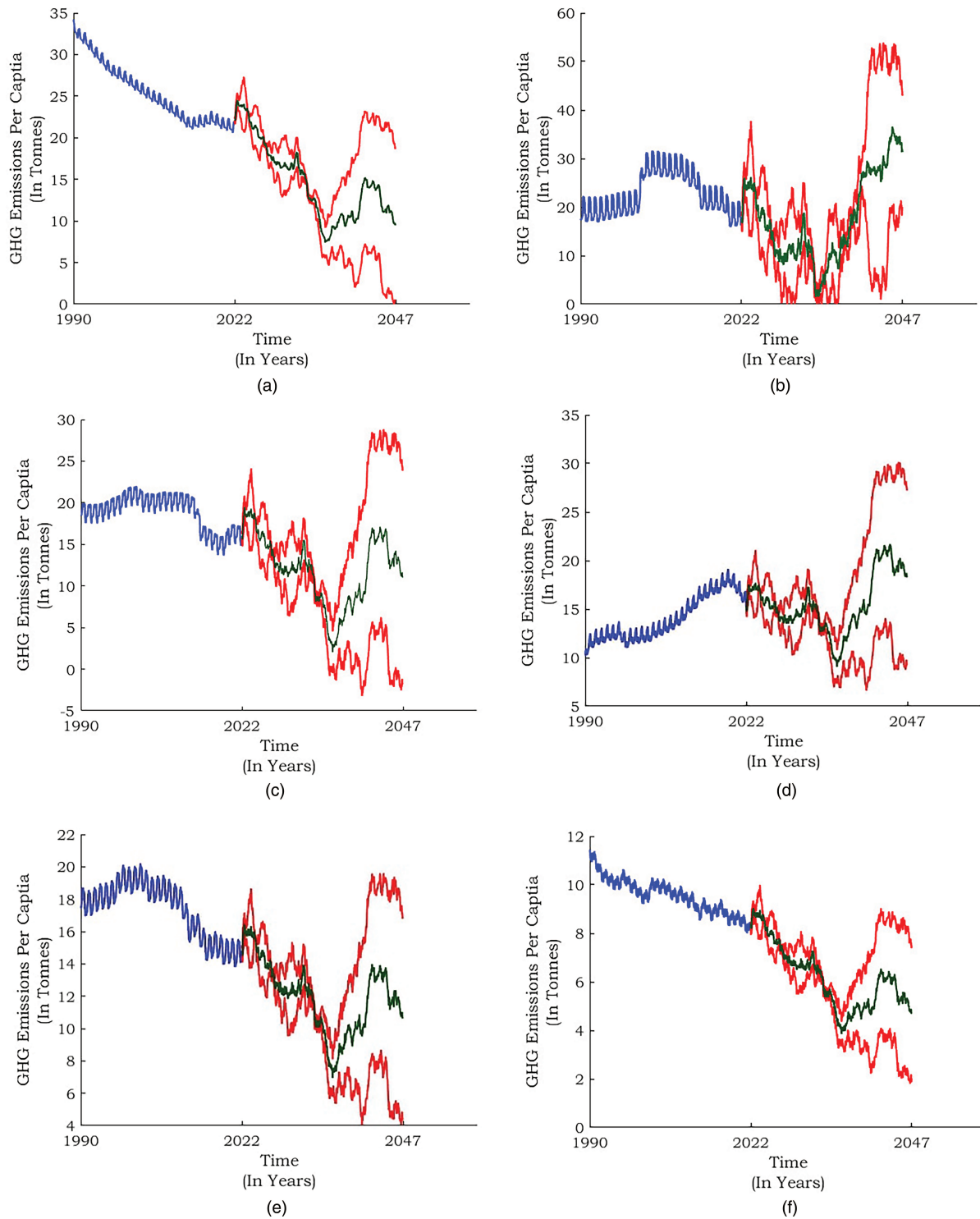
FIG. 13. Comparison of predicted per capita greenhouse gas emissions (in tons) from 2019 to 2047 using ARIMA (1,1,1) with scaling factors I_j^{**}: (a) Botswana, (b) Canada, (c) Australia, (d) Saudi Arabia, (e) USA, and (f) Germany.

However, after nearly four decades, the scale for interpreting the MAPE function, which is frequently employed in forecasting, has not been changed. The Lewis scale has been modified recently,[7] which relies on the assumption that time series forecasting has greatly upgraded over the past three decades to the point where a forecast is regarded inappropriate if at least one-third of the simulation is inappropriate. In the upgraded version, when the MAPE (%) value is less than 10, the forecast is highly accurate if it is between 10 and 20, the forecast is good, reasonable forecast when the MAPE (%) value is between 20 and 30, and the forecast is inaccurate if the MAPE (%) value is greater than or equal to 30. The root mean square error, also known as a root mean square deviation, is one of the most popularly used measures to evaluate the quality of predictions. It depicts the disparity between the predicted and observed true values. The formulation of RMSE is given by

$$\text{RMSE} = \sqrt{\frac{\sum_{j=1}^{N} \left(y(t_j) - \hat{y}(t_j)\right)^2}{N}}. \tag{8}$$

III. DATA DESCRIPTION

For the present study, the data on annual greenhouse gas emissions in three countries, China, US, India, and world, have been taken from the website Our World in Data.[17] The emission records from the year 1990–2018 is used for the investigation. The data of per capita greenhouse gas emissions of 11 countries, Botswana, Canada, Australia, Saudi Arabia, United States, Germany, Russia, China, United Kingdom, Brazil, and India, have also been taken from the website Our World in Data.[17] The principal sources of greenhouse gas emissions induced by human activity include energy (electricity, heat, and transport), direct industrial processes, waste, and land use (agriculture and forestry).

In the energy sector, 24.2% of greenhouse gases emit 7.2% from iron and steel, 3.6% from the chemical and petrochemical industries, and 12.6% from the other energy sources. 16.2% of indirect emissions are recorded owing to the burning of fossil fuels to promote transport activities. About 11.9% of emissions come from road transport and the rest from shipping, rail, and pipeline. Generation of electricity and heating in residential and commercial buildings lead to 17.5% of emissions. Unallocated fuel combustion and fugitive emissions from energy production contribute remaining percentage of emissions from the energy sector. In the industrial processes, cement production causes 3% of greenhouse gas emissions. Manufacturing of chemicals, such as plastic, pesticides, and fertilizers, contribute 2.2% of emissions. Wastewater treatment and landfills (low oxygen environments) emit 1.3% and 1.9% of greenhouse gases, respectively. Grassland (0.1%), cropland (1.4%), deforestation (2.2%), crop burning (3.5%), rice cultivation (1.3%), agricultural soils (4.1%), and livestock & manure (5.8%) are the subsectors that cause greenhouse gas emissions in the agriculture and forestry sector.

IV. RESULTS AND DISCUSSION

The greenhouse gas emissions (in tons) have been taken over the years, and a linear fractal interpolation function has been used to reconstruct the sample data points. Three distinct types of scaling

factors have been selected and compared with each other for the best approximation of the sample data. The autoregressive integrated moving average model, ARIMA (1,1,1), is employed to predict the future climatic conditions in long-term. Besides analyzing the predictions of annual GHG emissions in China, US, and India from 2019 to 2047, the per capita GHG emissions of 11 countries, namely, Botswana, Canada, Australia, Saudi Arabia, United States, Germany, Russia, China, United Kingdom, Brazil, and India, are also predicted from 2019 to 2047. The yearly emission rate of greenhouses gases (in tons) is illustrated in Fig. 4 from 1990 to 2020. Figure 4 clearly depicts the graphs of the total GHG emission rate of the three most emitting countries, China, US, and India. In Fig. 4, the blue curve, the red curve, and the green curve represent the fractal curves of GHG emissions in China, US, and India, respectively. In China, the emitting rate is not stable, and it tends to increase conspicuously for the ten years from 2003 to 2013. Though there is a slight fall in the curve during 2013–2017, the graph begins to rise after 2017. The emitting rate is gradually increasing in India, whereas the emitting rate fluctuates periodically with the time period in US. After 2005, the rate of GHG emissions in US shows a significant decrease until the end of 2018. The total GHG emission rates of China, US, and India are 12×10^9, 5×10^9, and 3×10^9 tons, respectively. Figure 5 represents the per capita greenhouse gas emissions of 11 countries, namely, Botswana, Canada, Australia, Saudi Arabia, United States, Germany, Russia, China, United Kingdom, Brazil, and India. Among the 11 countries, Botswana emits the highest rate of per capita GHG emissions. However, it follows a declining trend, and at the end of 2018, it the highest per capita GHG emitter globally. The per capita emission of Canada is nearly 17 tons at 1990. Later on, the curve gradually increases, and at the beginning of 2001, it achieves a peak. During 2002–2010, it is the highest GHG emitter globally, and then the curve gradually decreases and emits nearly 16 tons at 2018. Observing the curve of Australia, it falls down at the year 2010 and emits around 17 tons at 2018. The graph of the United States oscillates throughout the taken time period, and at the end of 2018, it emits around 16 tons of GHG. In Saudi Arabia, the emission rate starts to increase from 1997, and it keeps on increasing until 2015 and starts falling down and reaches 15 tons of per capita GHG emission. There is no much difference in the curve of Germany since the per capita emission rate is between 9 and 11 tons from 1990 to 2018. Similarly, the graph of the United Kingdom does not show much fluctuations until 2008, and then the graph declines and reaches 5 tons at the end. Comparing with the other ten countries, Russia shows greater fluctuations and emits nearly 7 tons at 2018, which is lesser than the emission rate at 1990. China's curve significantly increases without decline until 2018, and the per capita emission rate is more than 5 tons at 2018. It is observed that there is a drastic fall of Brazil curve from 7 to 3 tons during 2009–2011, and at the end of 2018, the per capita emission rate is around 4 tons. The graph of India constantly increases with no fluctuations, and the level of per capita emission is 3 tons, which indicates that India is the least per capita emitting country among the chosen 11 countries. The fractal curves in Fig. 6 are drawn by choosing the scaling factors l_j as proposed in the fractal interpolation–ARIMA algorithm. The red curves in Figs. 6–14 represent the lower bound and the upper bound of the predicted values (the rate of greenhouse gas emissions in tons). The predicted values (represented in green curves) are expected to lie in
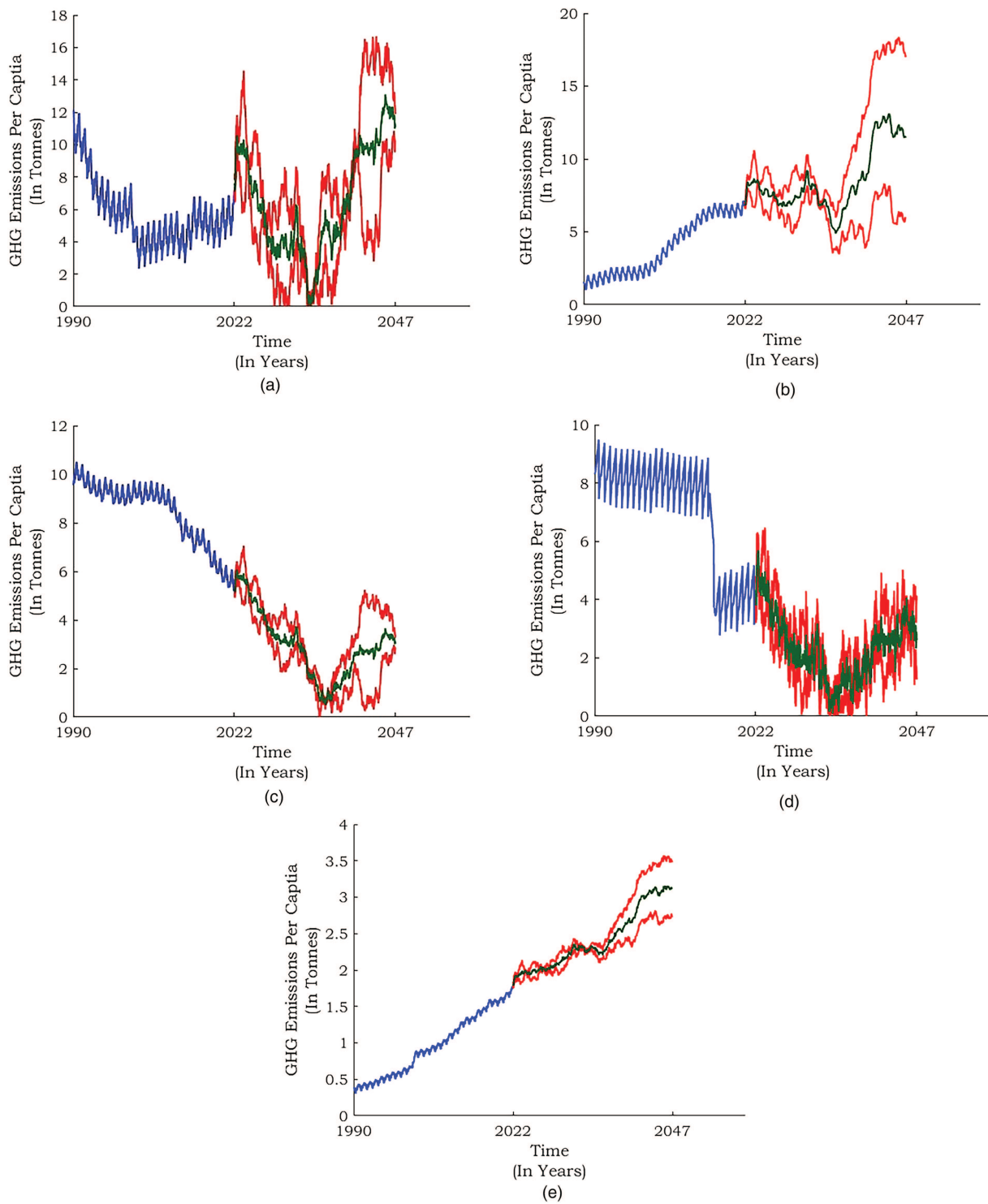
FIG. 14. Comparison of predicted per capita greenhouse gas emissions (in tons) from 2019 to 2047 using ARIMA (1,1,1) with scaling factors l_j^{**}: (a) Russia, (b) China, (c) UK, (d) Brazil, and (e) India.

between the deviated values (red curves). The range of possible predictions can be determined with the help of deviated values. In Fig. 7, the graphs are obtained by taking the scaling factor as chosen in the literature,[14] given by

$$l_j^* = \frac{y_j - y_{j-1}}{\delta\sqrt{(y_{max} - y_{min})^2 + (y_j - y_{j-1})^2}},$$

where $\delta = 1 + \text{rand}(\varepsilon)$ and $\text{rand}(\varepsilon)$ is the random number taken by the computer. On the other hand, the curves in Fig. 8 are generated by taking the scaling factors as constant, $l_j^{**} = 0.5$.

Figures 6(a)–6(d) illustrate the predicted GHG emissions in three countries: the China, United States, and India, and the world, respectively. The prediction is performed until 2047 using the ARIMA model. In comparison with China and India, the graph of the United States has more oscillations from 2019 to 2047, as shown in Fig. 6(b). The curve declines and the emission rate falls below 5×10^9 tons and begins to increase constantly until 2045, and then the curve falls again. The United States is expected to emit a maximum of 6.5×10^9 tons of greenhouse gases. The following causes account for the declining trend of GHG emissions in the United States.[30]

- From 1990 to 2007, emissions increased at roughly the same rate as the population, resulting in relatively stable emissions per capita. Between 2007 and 2009, total emissions and emissions per capita decreased, owing in part to a decrease in the US economic output. Emissions fell further between 2010 and 2012, owing largely to the increased use of natural gas to generate electricity rather than more carbon-intensive fuels.
- Carbon dioxide is absorbed from the atmosphere via emission sinks, which are the polar opposites of emission sources. Net sinks resulting from land use and forestry practices offset 12% of US greenhouse gas emissions in 2019.

GHG emissions in China and India do not follow a downward trend or fluctuate as they do in the United States. In China, the emission rate has been steadily increasing until 1995, and there is a constant level of emission up to 2015. Then, with a fall between 2016 and 2018, the forecasted graph shows an increasing trend until 2024. By the end of 2047, it is predicted that the emission rate will have surpassed 2×10^9 tons. India's curve continues to rise steadily until 2030, with no decline. The bend then takes a minor detour, and then the curve meets a slight fall. From 2035 onward, the curve steepens, and it is predicted that the India emits roughly 6×10^9 tons of greenhouse gases. China and India are anticipated to boost their greenhouse gas emissions during the next two decades. From Fig. 6(d), it is observed that the worldwide rate of greenhouse gas emissions fluctuates over time, taking into account both the past recorded and predicted data. The curve indicates that global GHG emissions are predicted to cross 6×10^9 tons by 2047.

Figure 9 demonstrates the predicted greenhouse gas emissions per capita of six countries, namely, Botswana, Canada, Australia, Saudi Arabia, United States, and Germany, from 2019 to 2047. Figure 10 shows the predicted greenhouse gas emissions per capita of five countries, namely, Russia, China, United Kingdom, Brazil, and India. The fractal curves in Figs. 9 and 10 are drawn using

the scaling factor l_j, which is proposed in the fractal interpolation–ARIMA algorithm. The predicted greenhouse gas emissions per capita of six countries, namely, Botswana, Canada, Australia, Saudi Arabia, United States, and Germany, are drawn using the scaling factor l_j^* and illustrated in Fig. 11. Similarly, by choosing the scaling factor as l_j^*, the per capita greenhouse gas emissions are predicted until 2047 for the countries, Russia, China, United Kingdom, Brazil, and India, and demonstrated in Fig. 12. Furthermore, by taking the scaling factor as l_j^{**}, the greenhouse gas emissions are predicted until 2047 for all the 11 countries and demonstrated in Figs. 13 and 14.

From Fig. 9(a), it is noticed that the graph of per capita GHG emissions of Botswana decreases gradually, and the curve does not fluctuate much. The emission rate is nearly 10 tons at 2047, which is 3 times lesser than the emission rate (35 tons) at 1990. The curve of Canada in Fig. 9(b) shows peaks at various time periods, and finally, the per capita emission rate is around 15 tons, which is more similar to the rate at 1990. The graphs of Australia and USA are analog to each other. Both the curves in Figs. 9(c) and 9(e) fall to 5 tons between 2035 and 2038, and the emission rate is around 12 tons at the end. From Fig. 9(d), Figs. 10(b) and 10(e), the curves of Saudi Arabia, China, and India increase from 1990, and the rates are 21, 12, and 3 tons, respectively, at 2047. Figure 9(f) shows that Germany's per capita GHG emissions rate declines with fluctuation, and finally, the emission rate is 4 tons. From Figs. 10(a) and 10(d), it is observed that the per capita emission rates of Russia and Brazil vanish at a certain period and then begin to rise. Figure 10(c) demonstrates that from 2022 onward, the curve of UK falls, and it is expected at the year 2047, the emission rate vanishes.

Table I evaluates the forecast errors of the ARIMA model through three evaluation metrics: MAPE, NMAPE, and RMSE. For three different types of scaling factors l_j (Model I), l_j^* (Model II), and l_j^{**} (Model III), the future greenhouse gas emissions are predicted. The evaluation metrics help to test the best approximation of prediction among the three models. As discussed in Secs. I–III, the forecast is reasonable if the MAPE value is closer to 0% and the forecast is imperfect if it is greater than 100%. From Table I, it is clear that the predictions of GHG emissions through Model I are reasonable forecasts for all the countries except China. The MAPE values of Model II show that the forecasts are perfect except the country, India, whereas in the case of Model III, the forecasts are good except India as like Model II. The forecast error of China and India is due to the reason that both their graphs tend to increase constantly without any fluctuations in Fig. 5. From the observed MAPE values, the forecast error in Model II is lesser for China and Brazil, while in Model II, it is lesser for Saudi Arabia, China, and Brazil. However, the forecast error of Model I is smaller for most of the 11 countries than the other two models. Hence, Table I confirms that the scaling factor proposed in this paper provides the best prediction of future GHG emissions. Furthermore, as the numbers in Table I demonstrate the goodness of each model, the lower the number, the better the model. As a consequence, the NMAPE and RMSE values show that the ARIMA model fits the sample better than the other two models. This result is very useful in predicting the future GHG emissions to avoid the worst impacts of the global climate dynamics.

V. CONCLUDING REMARKS

The present study forecasts the global greenhouse gas emissions through the ARIMA model. By making use of the past data on GHG emissions, future per capita GHG emission rates of 11 countries have been forecasted. Initially, the sample data have been reconstructed into finer data using the fractal interpolation and applying the ARIMA model, and the future GHG emissions are forecasted. The evaluation metrics, RMSE, MAPE, and NMAPE, are estimated to compare and find the best model out of the three models I, II, and III. They are calculated by taking the observed values as the original data and the estimated data as the preprocessed data using fractal interpolation. The original data are the same for all the three models discussed in the article. For Model I, the predicted data are obtained by preprocessing the original data using fractal interpolation with the scaling factor l_j. For Models II and III, the same procedure is repeated only by changing the scaling factors as l_j^* and l_j^{**}, respectively. It is found out from the evaluation that our proposed model (model I) gives the best approximation, and the extrapolation is done for predicting the future emissions with the preprocessed data using the ARIMA model. It is observed that the forecast error of almost all the countries converges to zero except China and India. Hence, it is concluded that the results produced in this study are realistic and sensible for the maximum number of countries in predicting the future climate dynamics. Furthermore, it is estimated that the world level GHG emission rate would be more than 6 tons at the end of 2047. As the activities of human rise, GHG builds up in the atmosphere, warming the weather and causing plenty of other changes in the atmosphere, on the land, and in the seas. Since several major greenhouse gases remain in the atmosphere for hundreds of years after release, their warming impacts on the climate last for a long time, affecting both the present and future generations. Though the emissions of GHG are stopped, their associated global warming and sea-level rise would continue for more than 100 years. This study alerts that short-lived greenhouse gases affect decades of sea-level rise. Thus, to avoid future sea-level rise and submerge of the world, greenhouse gas emissions must be reduced.

ACKNOWLEDGMENTS

AUTHOR DECLARATIONS
Conflict of Interest

The authors have no conflicts to disclose.

Author Contributions

A. Gowrisankar: Formal analysis (equal). **T. M. C. Priyanka:** Writing – original draft (equal). **Asit Saha:** Validation (equal). **Lamberto Rondoni:** Investigation (equal); Validation (equal). **Md. Kamrul Hassan:** Validation (equal). **Santo Banerjee:** Conceptualization (equal).

DATA AVAILABILITY

The data that support the findings of this study are openly available in Our World in Data at https://ourworldindata.org/co2-and-other-greenhouse-gas-emissions, Ref. 17.

REFERENCES

[1] T. S. Ledley, E. T. Sundquist, S. E. Schwartz, D. K. Hall, J. D. Fellows, and T. L. Killeen, "Climate change and greenhouse gases," Eos **80**, 453–458 (1999).
[2] J. F. B. Mitchell, "The greenhouse effect and climate change," Rev. Geophys. **27**, 115–139, https://doi.org/10.1029/RG027i001p00115 (1989).
[3] Z. Ren, G. Foliente, W.-Y. Chan, D. Chen, M. Ambrose, and P. Paevere, "A model for predicting household end-use energy consumption and greenhouse gas emissions in Australia," Int. J. Sustain. Build. Technol. Urban Dev. **4**, 210–228 (2013).
[4] S. V. Jørgensen, M. Z. Hauschild, and P. H. Nielsen, "Assessment of urgent impacts of greenhouse gas emissions—The climate tipping potential (CTP)," Int. J. Life Cycle Assess. **19**, 919–930 (2014).
[5] T. K. Loan Nguyen, H. H. Ngo, W. Guo, T. L. Hong Nguyen, S. W. Chang, D. D. Nguyen, S Varjani, Z. Lei, and L. Deng, "Environmental impacts and greenhouse gas emissions assessment for energy recovery and material recycle of the wastewater treatment plant," Sci. Total Environ. **784**, 147135 (2021).
[6] J. G. Titus, "Greenhouse effect, sea level rise and land use," Land Use Policy **7**, 138–153 (1990).
[7] S. A. Javed and D. Cudjoe, "A novel grey forecasting of greenhouse gas emissions from four industries of China and India," Sustain. Prod. Consum. **29**, 777–790 (2022).
[8] R. Yang and B. Xing, "A comparison of the performance of different interpolation methods in replicating rainfall magnitudes under different climatic conditions in Chongqing Province (China)," Atmosphere **12**, 1318 (2021).
[9] S. Wan, Q. Liu, J. Zou, and W. He, "Nonlinearity and fractal properties of climate change during the past 500 years in Northwestern China," Discrete Dyn. Nat. Soc. **2016**, 4269431.
[10] C. Masciopinto and I. S. Liso, "Assessment of the impact of sea-level rise due to climate change on coastal groundwater discharge," Sci. Total Environ. **569–570**, 672–680 (2016).
[11] G. Rangarajan and D. Sant, "Fractal dimensional analysis of Indian climatic dynamics," Chaos, Solitons Fractals **19**, 285–291 (2004).
[12] L. Xin-Fu and L. Xiao-Fan, "An explicit fractal interpolation algorithm for reconstruction of seismic data," Chin. Phys. Lett. **25**, 1157 (2008).
[13] G. Althor, J. E. M. Watson, and R. A. Fuller, "Global mismatch between greenhouse gas emissions and the burden of climate change," Sci. Rep. **6**, 20281 (2016).
[14] X. Liu, C. Xia, Z. Chen, Y. Chai, and R. Jia, "A new framework for rainfall downscaling based on EEMD and an improved fractal interpolation algorithm," Stoch. Environ. Res. Risk Assess. **34**, 1147–1173 (2020).
[15] S. Y. Ming Xie, L. Wu, L. Liu, Y. Bai, L. Liu, and Y. Tong, "A novel robust reweighted multivariate grey model for forecasting the greenhouse gas emissions," J. Clean. Prod. **292**, 126001 (2021).
[16] Z. Ming-Yue, H. Kuzumab, and J. W.. Rector, "A new fractal algorithm to model discrete sequences," Chin. Phys. B **19**, 090509 (2010).
[17] H. Ritchie, M. Roser, and P. Rosado (2020). "CO$_2$ and greenhouse gas emissions," Our World in Data. https://ourworldindata.org/co2-and-other-greenhouse-gas-emissions
[18] H.-Y. Wang, H. Li, and J.-Y. Shen, "A novel hybrid fractal interpolation-SVM model for forecasting stock price indexes," Fractals **27**, 1950055 (2019).
[19] S. Raubitzek and T. Neubauer, "A fractal interpolation approach to improve neural network predictions for difficult time series data," Expert Syst. Appl. **169**, 114474 (2021).
[20] C. Xiu, T. Wang, M. Tian, Y. Li, and Y. Cheng, "Short-term prediction method of wind speed series based on fractal interpolation," Chaos, Solitons Fractals **68**, 89–97 (2014).
[21] A. Gowrisankar, T. M. C. Priyanka, and S. Banerjee, "Omicron: A mysterious variant of concern," Eur. Phys. J. Plus **137**, 100 (2022).

[22]M. F. Barnsley, "Fractal functions and interpolation," Constr. Approx. **2**, 303–329 (1986).

[23]M. F. Barnsley, *Fractals Everywhere* (Academic Press, 1993).

[24]D. Easwaramoorthy and R. Uthayakumar, "Analysis of biomedical EEG signals using wavelet transforms and multifractal analysis," in *IEEE International Conference on Communication Control and Computing Technologies* (IEEE, 2010), pp. 544–549.

[25]S. Banerjee, D. Easwaramoorthy, and A. Gowrisankar, *Fractal Functions, Dimensions and Signal Analysis* (Springer, Cham, 2021).

[26]A. P. García-Marín, J. Estévez, J. A. Alcalá-Miras, R. Morbidelli, A. Flammini, and J. L. Ayuso-Muñoz, "Multifractal analysis to study break points in temperature data sets," Chaos **29**, 093116 (2019).

[27]T. M. C. Priyanka and A. Gowrisankar, "Analysis on Wely-Marchaud fractional derivative of types of fractal interpolation function with fractal dimension," Fractals **29**, 1157 (2021).

[28]T. M. C. Priyanka and A. Gowrisankar, "Riemann–Liouville fractional integral of non-affine fractal interpolation function and its fractional operator," Eur. Phys. J. Spec. Top. **230**, 3789–3805 (2021).

[29]S. T. Ogunjo, I. Fuwape, A. Babatunde Rabiu, and S. S. Oluyamo, "Multifractal analysis of air and soil temperatures," Chaos **31**, 033110 (2021).

[30]See https://www.epa.gov/climate-indicators/climate-change-indicators-us-greenhouse-gas-emissions for information about U.S. Greenhouse Gas Emissions.